THE ANNALS OF "DUNAREA DE JOS" UNIVERSITY OF GALATI
FASCICLE IX. METALLURGY AND MATERIALS SCIENCE
N^0. 3 – 2014, ISSN 1453 – 083X

STRUCTURAL CHANGES ASSOCIATED WITH THE PSEUDOELASTIC RESPONSE OF Fe-BASED SHAPE MEMORY ALLOYS

Bogdan PRICOP[1], Nicoleta Monica LOHAN[1], Firuța BORZA[2], Nicoleta LUPU[2], Marius-Gabriel SURU[1], Elena MIHALACHE[1], Radu Ioachim COMĂNECI[1], Leandru-Gheorghe BUJOREANU[1*]

[1]Faculty of Materials Science and Engineering, "Gheorghe Asachi" Technical University of Iaşi
61A, Avenue D. Mangeron, 700050 Iaşi, Romania
[2]National Institute of Research and Development for Technical Physics,
47 Avenue Mangeron, 700050, Iaşi, Romania
* Corresponding author
e-mail: lgbujor@tuiasi.ro

ABSTRACT

The pseudoelastic responses of two types of iron base shape memory alloys (SMAs) were introduced and discussed. The former was based on Fe-Mn-Si system, obtained by classical (CM) and by powder metallurgy (PM) manufacturing. The latter was based on Fe-Ni-Co system being processed by a non conventional technology comprising melt spinning and heat treatment. In the case of FeMnSi-based SMAs, CM specimens obviously experienced larger ductility and a more pronounced pseudoelastic response while PM specimens were stiffer and underwent larger work-hardening. On the other hand, melt spun FeNiCo-based SMAs revealed an outstanding superelasticity in the case of micro-indentation tests. By means of scanning electron microscopy (SEM) observations, a martensitic morphology was identified in FeMnSi-based SMAs while FeNiCo-based SMAs revealed an austenitic structure. The presence of both α' and ε martensites was confirmed in FeMnSi-based SMAs by means of X-ray diffraction (XRD). In fully austenitic melt-spun and aged FeNiCo-based SMAs, no martensite was indentified on XRD patterns. These results sustain the conclusion that FeMnSi-based SMAs, that contain pre-existing martensite, experienced a pseudoelastic behavior caused by crystallographic reorientation of martensite plate variants while austenitic FeNiCo-based SMAs experienced a reversible stress-induced martensitic transformation, at room temperature.

KEYWORDS: shape memory alloys, pseudoelasticity; tensile tests; micro-indentation; superelasticity, stress induced martensite

1. Introduction

Shape memory alloys (SMAs) are metallic materials exhibiting the ability to return to some previously defined shape or size when subjected to an appropriate thermal or mechanical procedure, a response that characterizes the so-called "thermal memory" or "mechanical memory" respectively [1]. These two different types of memory responses are illustrated by one way and two way effects (1-WE, 2-WE) and by superelastic behavior, respectively [2].

In general, pseudoelasticity (PE) represents any additional spring back on the elastic unloading portion of a force-displacement curve [3], while superelasticity (SE) is a particular form of PE associated with the presence of a stress plateau on the unloading portion of an isothermal stress-strain curve, caused by a reversible stress-induced martensitic transformation [4].

Iron-based SMAs have been extensively studied in the last years due to their promising results concerning mostly their thermal memory behavior and less their superelastic behavior [5]. Thus, FeMnSi-based SMAs cannot develop SE responses [6] in spite of cumbersome thermo-mechanical training processes meant to improve the shape

memory and superelastic properties [7]. Partial PE was observed in FeMnSi-based SMAs, being associated with incomplete γ (face centre cubic, fcc) → ε (hexagonal close-packed, hcp) stress-induced martensitic transformation (MT) that was slightly enhanced by pre-strain increase up to 8% [8]. The PE response of the FeMnSi-based SMAs is incomplete, since the deformation above reverse martensitic transformation temperatures induces slip deformation due to the large temperature hysteresis [9].

On the other hand, in FeNiCo-based SMAs the precipitation of the disperse $(CoNi)_3Ti$ particles with $L1_2$-type atomic-ordered structure results in a change of the kinetics of γ (fcc)−α′ (body centre cubic, bcc) MT from a non-thermoelastic kinetics with large temperature hysteresis H = 400 K to a γ (fcc)−α′ (body centre tetragonal, bct) thermoelastic one with the hysteresis H ~ 30–100 K in the heterophase state [10]. $(CoNi)_3Ti$ particles, designated as γ' precipitates, do not undergo martensitic transformation, but in turn they favor the accumulation of the elastic energy in martensite crystals, thus causing a back stress which enhances martensite reversion to parent phase (austenite) [11]. Concerning FeNiCo-based SMAs a remarkable result was recently reported by Tanaka *et al.* who developed a polycrystalline FeNiCoAlTaB alloy characterized by a superelastic response that was never observed in polycrystalline SMAs [12]. Due to the superelastic strain of more than 13%, presented by Tanaka *et al.* correlated with a tensile strength above 1 GPa, the SE response obtained in highly textured FeNiCo-based SMAs authorized the term "huge superelasticity" to be used for the first time in association with SMAs [13]. The present paper aims to compare the pseudoelastic responses of a FeMnSi-based and a FeNiCo-based SMA, obtained by different manufacturing technologies, and to corroborate these responses with the structures of the respective alloys.

2. Experimental procedure

An Fe-18Mn-3Si-7Cr-4Ni (mass. %) SMA was produced by classical metallurgy (CM) and by powder metallurgy (PM), using high frequency induction melting, pressing and sintering at 1390 K. Mechanical alloying (MA) was applied in order to attained compositional homogenization of FeMnSi-based SMAs [14] and for this purpose a ball to powder ratio (BPR) of 1/8 and a 2 mass. % fraction of Stearic Acid (SA) were used [15]. After homogenization annealing, (1370 K/ 1 hr. /water) specimens' thickness was reduced to about 1×10^{-3} m by hot rolling, at 1270 K. Both CM and PM specimens, cut to $1 \times 5 \times 40 \times 10^{-3}$ m, were subjected to tensile loading-unloading tests on an INSTRON 3382 tensile testing machine with a deformation rate of 2.77×10^{-4} sec^{-1}.

After embedding into cold mounting resin and metallographic preparation, SEM analysis was conducted on a SEM - VEGA II LSH TESCAN scanning electron microscope (SEM), coupled with an EDX - QUANTAX QX2 ROENTEC detector. X-ray diffraction (XRD) patterns were recorded on a BRUKER AXS D8 Advance diffractometer with Cu K_α [16].

$Fe_{40.95}Ni_{28}Co_{17}Al_{11.5}Ta_{2.5}B_{0.05}$ ribbons, with cross-section of $43 \times 70 \times 10^{-6}$ m, were prepared by melt spinning and were aged for 2× 3.6 ks at 923 K. Micro-indentation tests were performed with a sharp indenter, on a UMT-CETR universal tester at a maximum load of 15 N. Load-depth indentation curves were recorded, at a position precision of 1×10^{-7}m, by means of the CETR data viewing software.

Embedded ribbons were observed by means of a JEOL JSM 6390 SEM microscope and analyzed on a D8 Advance - Bruker AxS GmbH diffractometer with Cu-K_α radiation, radiation intensity I_e=40mA and Voltage= 40KV [17].

3. Results and discussion

Two stress-strain curves obtained during two successive loading-unloading tensile tests of CM Fe-18Mn-3Si-7Cr-4Ni SMA specimens are illustrated in Fig. 1.

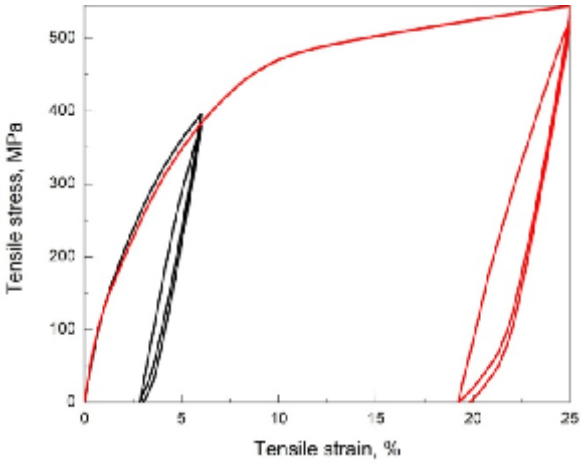

Fig. 1. *Stress-strain curves, recorded on two specimens of Fe-18Mn-3Si-7Cr-4Ni (mass. %) SMA processed by classical metallurgy. Two loading-unloading tensile tests were performed up to 5% and to 25% total strains, respectively, in order to illustrate the augmentation tendency of PE response with the increase of total strain*

The loading portions reveal rounded plastic regions, characteristic for transformation induced plasticity (TRIP) [18], which are visible only during first loading. This change suggests that stress induced martensitic transformation is the governing deformation mechanism only during first loading while slip becomes prominent during subsequent loadings. On the other hand, in both cases unloading has been accompanied by a PE response. Considering the values of pseudoelastic strain (ε_{pe}) as the difference between unloading recovery strain (ε_{rec}) and elastic strain (ε_e) [8], it follows that for 5% the total strain is ε_{pe} = 2.8 - 2.4 = 0.4% while for 25% total strain is ε_{pe} = 5.2 - 3.7 = 1.5%, which suggests that PE response tends to increase with total strain.

In the case of PM Fe-18Mn-3Si-7Cr-4Ni SMA, total strain could not exceed 4%. However, TRIP-characteristic deformation behavior during first loading has also been noticeable in the case of PM specimens, as shown in the representative tensile stress-strain curves illustrated in Fig. 2.

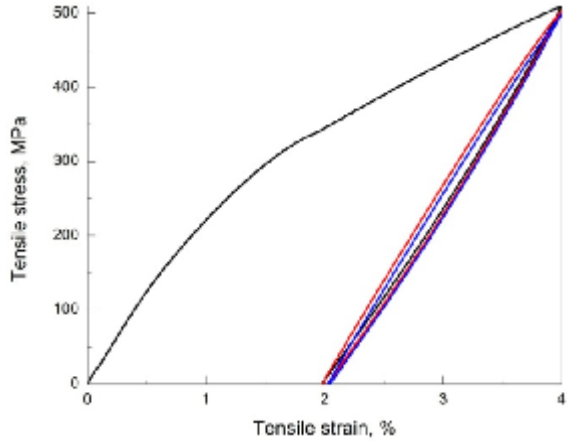

Fig. 2. *Stress-strain curves, recorded on a specimen of Fe-18Mn-3Si-7Cr-4Ni (mass. %) SMA processed by powder metallurgy with mechanical alloying. Three loading-unloading tensile tests were performed up to 4% total strain which illustrate a slight diminution tendency of PE response with the increase of the number of cycles*

As compared to CM specimens, PM specimens revealed less marked TRIP behavior and less PE response, yet higher strength and stiffness. With increasing the number of cycles, pseudoelastic strain decreased from 0.37% in the first cycle, to 0.34% in the second and to 0.33% in the third, in good agreement with the general decreasing tendency with increasing the number of loading-unloading cycles, previously reported in the variation of strain recovery degree of PM FeMnSi-based SMAs [19].

These hardening effects could be caused by mechanical alloying (MA) which, in the case of low-Mn Fe-based alloys, enhances deformation hardening due to the formation of brittle α' martensite [20]. In addition, since TRIP effect is mainly caused by stress-induced formation of ε –hcp martensite [21], it is expectable that PM FeMnSi-based specimen contains less amount of this phase.

A different insight into the PE and SE responses of the FeMnSi-based and FeNiCo-based alloys under study is given by micro-indentation tests. Figure 3 illustrates the micro-indentation curve of CM FeMnSi-based SMA.

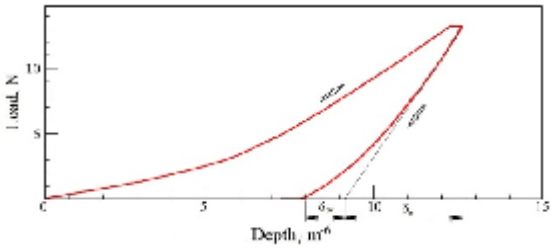

Fig. 3. *Micro-indentation curve of Fe-18Mn-3Si-7Cr-4Ni (mass. %) SMA processed by classical metallurgy illustrating a PE response characterized by 38.1% recoverable penetration depth and 10.3% pseudoelastic penetration depth*

In contrast to spherical-indenter tests [22], the micro-indentation curve from Fig. 3 reveals a notable PE response. Considering that reversible stress-induced phase transition mechanisms require the presence, on the unloading stage of indentation curves, either of load plateaus or of "pop-out events" [23], it is obvious, from Fig. 3, that none of these events is noticeable. Therefore, during indentation tests, in good agreement with tensile stress-strain curves shown in Fig. 1, it can be considered that stress-induced formation of martensite is irreversible in CM FeMnSi-based SMA under study. The change of the slope in Fig. 3 suggests a change in the deformation mode, form stress-induced formation of martensite in the lower part, to dislocation slip, corresponding to the upper part of indentation curve, according to similar results obtained at FeMnSi-based SMAs [24]. By determining the values of recovery depth and elastic depth as $\delta_{rec} = 4.8 \times 10^{-6}$ m and $\delta_e = 3.5 \times 10^{-6}$ m, respectively it follows that pseudoelastic penetration depth has the value $\delta_{pe} = \delta_{rec} - \delta_e = 1.3 \times 10^{-6}$ m. The PE response of CM FeMnSi-based SMA can be expressed, as percentages of total penetration depth of 12.6×10^{-6} m.

Thus, recoverable depth (δ_{rec}) represents 38.1% and pseudoelastic depth (δ_{pe}) only 10.3%.

A different micro-indentation curve was recorded in the case of melt spun and aged FeNiCo-based SMA ribbons, as shown in Fig. 4.

The load plateau noticeable on the unloading portion of micro-indentation curve upholds the reversible character of stress-induced martensitic transformation, characteristic to superelastic behavior in two-phase region, of FeNiCo-based SMAs [25]. In this case, considering total indentation depth as 19.7 × 10^{-6} m and permanent indentation depth 8.6 × 10^{-6} m, it follows that recovery indentation depth is δ_{rec} = 11.1 × 10^{-6} m. In this case elastic indentation depth is δ_e = 2.3 × 10^{-6} m and pseudoelastic indentation depth becomes δ_{pe} = 8.8 × 10^{-6} m. As compared to total indentation depth, recovery depth represents 11.1/19.7 × 100 = 56.3% while pseudoelastic depth is 8.8/19.7 × 100 = 44.6%. These values justify the use of SE response instead of PE response in relation to FeNiCo-based SMAs.

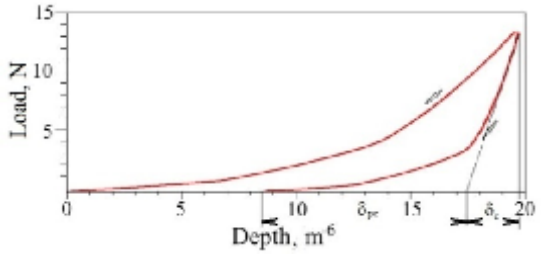

Fig. 4. *Micro-indentation curve of melt spun $Fe_{40.95}Ni_{28}Co_{17}Al_{11.5}Ta_{2.5}B_{0.05}$ aged for 2 × 3.6 ks at 923 K illustrating a SE response characterized by 56.3% recoverable penetration depth and 44.6% pseudoelastic penetration depth*

From the structural point of view, CM FeMnSi-based SMAs reveal martensite plates in an austenite matrix, as illustrated in Fig. 5, by means of representative SEM micrograph.

The triangle morphology, typical to ε - hcp martensite [26], is hardly noticeable on the micrograph shown in Fig. 5, thus suggesting that most of martensite plates would belong to α'-bct martensite, which is common presence in low-manganese FeMnSi-based SMAs [27].

A typical SEM micrograph of the surface of melt spun and aged FeNiCo-based SMA ribbons is presented in Fig.6.

The micrograph shows a fully austenitic structure [25] with an average grain size of approximately 10 micrometers [17]. Some of austenite grains contain parallel bands which can be identified as twins. White-color dispersed particles, with an average size estimated to 90 nanometers, were identified by energy dispersive X-ray (EDX) measurements as Ta.

The total absence of martensite plates, which are indispensable for a FeNiCo-based SMA alloy to exhibit shape memory effect (SME), supports the assumption that α'-bct martensite cannot be stabilized at room temperature [28]. In good accordance with the SE response observed in Fig. 5, it can be assumed that α'-bct stress-induced martensite formed from austenite during loading and, being unstable, reverted to austenite during unloading [29].

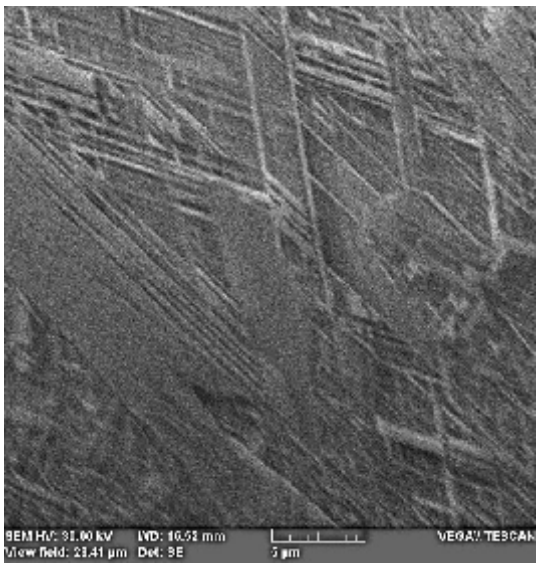

Fig. 5. *Typical SEM micrograph of Fe-18Mn-3Si-7Cr-4Ni (mass. %) SMA processed by classical metallurgy revealing multivariant martensite plates in a matrix of retained austenite*

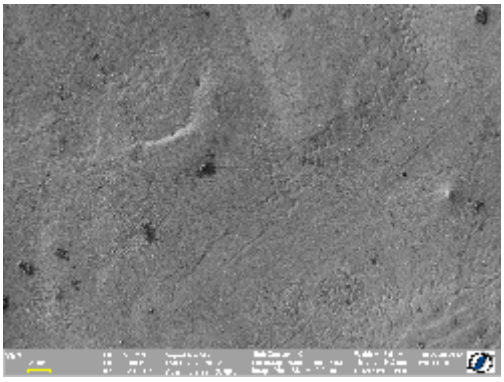

Fig. 6. *Typical SEM micrograph of melt spun $Fe_{40.95}Ni_{28}Co_{17}Al_{11.5}Ta_{2.5}B_{0.05}$ aged for 2 × 3.6 ks at 923 K revealing fully austenitic structure with twins*

A proper identification of phase structure of the two alloys under study was performed by XRD. The first representative XRD patterns for FeMnSi-based SMAs under study are shown in Fig. 7.

It is obvious that the amount of ε - hcp martensite is very low since, in PM specimen, the main diffraction maximum $(10\bar{1}1)$ is absent and the only basal plane, (0002), is present with a very low intensity. This coexistence of the two types of martensite can be a consequence of the complex thermal phenomena prone to occur in powder mixtures of mechanically alloyed particles, such as magnetic transition of Ni, glass-transition of amorphous regions and surface oxidation, only α'-bct is noticeable [30]. Normally, the amount of ε - hcp martensite should markedly increase after a tensile loading-unloading cycle [31]. In initial state, the structure of PM FeMnSi-based SMA specimen contains an approximate amount of 10.5% ε - hcp martensite. Conversely, the amount of α'-bct martensite can be estimated around 17.4% in PM specimen and 15.2% in CM specimen. The larger amount of martensite, pre-existing in PM specimen can be the cause of its higher stiffness.

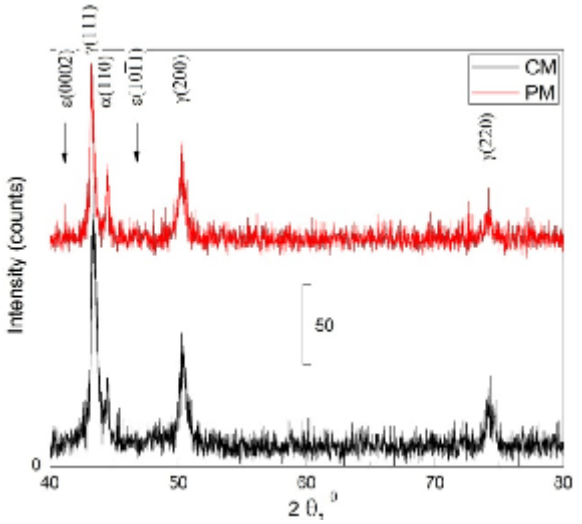

Fig. 7. *Representative XRD patterns for Fe-18Mn-3Si-7Cr-4Ni (mass. %) SMA processed by classical metallurgy (CM) and by powder metallurgy (PM)*

As expected, the structure of melt spun and aged FeNiCo-based ribbons are fully austenitic with γ' precipitates, as resulting from the XRD - pattern shown in Fig. 8.

The inset gives a detail of the diffraction peak of γ'-phase, meant to harden austenitic matrix in such a way as to give martensitic transformation a thermoelastic character [32]. The amount of γ'-phase was estimated to approx. 11.7% but, due to its nanometric size [7, 13, 29], the precipitates cannot be observed by SEM [33].

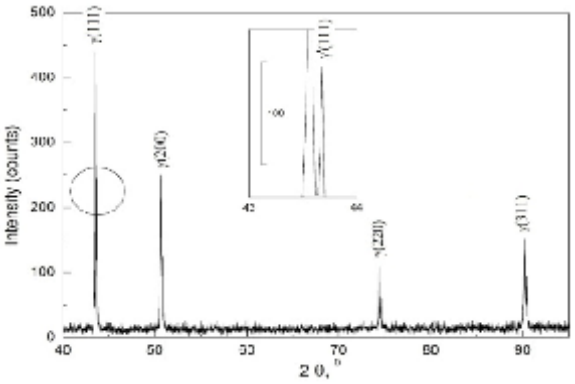

Fig. 8. *Representative XRD patterns for melt spun $Fe_{40.95}Ni_{28}Co_{17}Al_{11.5}Ta_{2.5}B_{0.05}$ aged for 2 × 3.6 ks at 923 K with inset detail of γ' diffraction peak*

4. Conclusions

The differences in the pseudoelastic behavior of two Fe-based SMAs were associated with:

- the pre-existence of martensite in a classical metallurgy processed FeMnSi-based specimen which experienced a pseudoelastic response of 1.5% in tension and of 10.3% at micro-indentation tests;
- the reversible stress-induced formation of martensite in melt spun and aged ribbons of FeNiCo-based SMA which experienced a superelastic response of 44.6% at micro-indentation tests.

Acknowledgement

This research work was supported by the project PN-II-ID-PCE-2012-4-0033, contract 13/2013.

References

[1]. Hodgson D. E., Ming H. W., Biermann R. J. - *Properties and Selection: Nonferrous Alloys and Special-Purpose Materials*, ASM Handbook, Vol. 2, (ASM International), 1990, p. 897-902.
[2]. Sun L., Huang W. M., Ding Z., Zhao Y., Wang C. C., Purnawali H., Tang C. - Mater Design, 33 (2012), p. 577-640.
[3]. Duerig T. W., Zadno R., *Engineering Aspects of Shape Memory Alloys*, edited by Duerig T W, Melton K N, Stöckel D, Wayman C M, (Butterworth-Heinemann) 1990, p. 369-393.
[4]. Wasilewski R. J. - *Shape Memory Effects in Alloys*, edited by Perkins J, (Plenum Press, New York-London), 1975, p. 245-271.
[5]. Dunne D. - *Phase transformations in steels: Diffusionless transformations, high strength steels, modelling and advanced analytical techniques*, Vol. 2, edited by Pereloma E & Edmonds D V, (Woodhead Publishing), 2012, p. 83-125.
[6]. Xiao-Xiang Wang, Chu-Yang Zhang - *J Mater Sci Letters*, 17 (1998), p. 1795-1796.
[7]. Ma J., Kockar B., Evirgen A., Karaman I., Luo Z. P., Chumlyakov Y. I. - *Acta Mater,* 60, 2012, p. 2186-2195.

[8]. Zhao C. - *J Mater Sci Letters,* 19, 2000, p. 1711 – 1713.
[9]. Sawaguchi T., Kikuchi T., Kajiwara S. - *Smart Mater Struct,* 14, 2005, p. S317-S322.
[10]. Chumlyakov Y. I., Kireeva I. V., Panchenko E. Y., Aksenov V. B., Kirillov V. A., Ovsyannikov A. V., Zakharova E. G., Sehitoglu H. - *Russ Phys J.*, 46 (8), 2003, p. 811-823.
[11]. Chumlyakov Y. I., Kireeva I. V., E. Panchenko Y., Zakharova E. G., Kirillov V. A., Efimenko S. P., Sehitoglu H. - *Dokl Phys*, 49 (1), 2004, p. 47-50.
[12]. Ma J., Karaman I. - *Science*, 327, 2010, p. 1468-1469.
[13]. Tanaka Y., Himuro Y., Kainuma R., Sutou Y., Omori T., Ishida K. - *Science*, 327, 2010, p. 1488-1490.
[14]. Söyler A. U., Özkal B., Bujoreanu L. G. - *Sintering Densification and Microstructural Characterization of Mechanical Alloyed Fe-Mn-Si based Powder Metal System*, Supp. Proc.TMS, 3, 2010, p. 785-792.
[15]. Söyler A. U., Özkal B., Bujoreanu L. G. - *Investigation of Mechanical Alloying Process Parameters on Fe-Mn-Si Based System*, Supp. Proc. TMS, 1, 2010, p. 577-583.
[16]. Bujoreanu L. G., Stanciu S., Ozkal B., Comaneci R. I., Meyer M. - ESOMAT 2009, 05003, 2009.
[17]. Paraschiv A. L., Suru M. G., Lohan N. M., Pricop B., Bujoreanu L. G., Borza F., Lupu N. - *Factors influencing the structure and proprieties of polycrystalline magnetic Fe-Ni-Co-Al-Ta-B shape memory alloy*, Proceedings of the International Conference on Shape Memory and Superelastic Technologies May 20–24, 2013, Prague, Czech Republic, p. 27-28.
[18]. Gu N., Lin C., Song X., Peng H., Yin F., Liu Q. - *Mater Sci Forum*, 327-328, 2000, p. 231-234.
[19]. Pricop B., Söyler U., Comăneci R. I., Özkal B., Bujoreanu L. G. - *Phys Proced*, 10, 2010, p. 125-131.
[20]. Cherdyntsev V. V., Pustov L. Y., Kaloshkin S. D., Tomilin I. A., Shelekhov E. V., Laptev A. I., Baldokhin Y. V., Estrin E. I. - *Phys Met Metallogr*, 104(4), 2007, p. 408-414.
[21]. Guo Y.-M., Wang G.-X., Feng J.-H., Chen C.-X., Peng H.-F. - *J Iron Steel Res Int*, 23(9), 2011, p. 50-54.
[22]. Wenyi Yan, Qingping Sun, Xi-Qiao Feng, Linmao Qian - *Int J Solids Struct,* 44, 2007, p. 1-17.
[23]. Maletta C., Furgiuele F., Sgambitterra E., Callisti M., Mellor B. G., Wood R. J. K. - *Frattura ed Integrità Strutturale*, 21 2012, p. 5-12.
[24]. Sekido K., Ohmura T., Sawaguchi T., Koyama M., Park H. W., Tsuzaki K. - *Scripta Mater,* 65, 2011, p. 942-945.
[25]. Titenko A. N., Demchenko L. D. - *J Mater Eng Perform*, 21, 2012, p. 2525-2529.
[26]. Sawaguchi T., Bujoreanu L.-G., Kikuchi T., Ogawa K., Yin F. - *ISIJ Inter*, 48(1), 2008, p. 99-106.
[27]. B. Pricop, U. Söyler, B. Özkal, N. M. Lohan, A. L. Paraschiv, M. G. Suru, L. G. Bujoreanu - *Mater Sci Forum*, 738-739, 2013, p. 237-241.
[28]. Sagaradze V. V., Kabanova I. G., Kataeva N. V., Klyukina M. F. - *Mater Sci Forum*, 738-739, 2013, p. 200-205.
[29]. Yonghong Geng, Mingjiang Jin, Wenjing Ren, Weimin Zhang, Xuejun Jin - *J Alloy Compd*, 2012, doi:10.1016/j.jallcom.2012.03.033.
[30]. Pricop B., Söyler U., Lohan N. M., Özkal B., Chicet D., David A., Bujoreanu L. G. - *Optoelectron Adv Mat*, 5(5), 2011, p. 555-561.
[31]. Bouraoui T., Jemal F., Ben Zineb T. - *Strength Mater*, 40(2), 2008, p. 203-211.
[32]. Hayashi R., Murray S. J., Marioni M., Allen S. M. O'Handley R. C. - *Sensors Actuat A*, 81, 2000, p. 219–223.